Modeling of glass reinforced matrices by the Coupled Criterion and the Matched Asymptotics Approach. The role of a single platelet

S Jiménez-Alfaro, D Leguillon

Modeling of glass matrix composites by the Coupled Criterion and the Matched Asymptotics approach. The role of a single platelet.

S. Jiménez-Alfaro[a,*], D.Leguillon[a]

[a]*Institut Jean Le Rond d'Alembert, Sorbonne Université – CNRS UMR 7190, 4 place Jussieu, 75000 Paris, France*

Abstract

The fracture toughness of glass is increased by the introduction of reinforced platelets made of a second constituent with high modulus, strength and/or ductility. In such composites different toughening mechanisms appear. In particular, the borosilicate glass/Al_2O_3 platelet composite introduced in 1996 is a very attractive solution for industrial purposes, since it is a environmentally friendly and low-cost material. In this paper the toughening mechanisms that correspond to a change in the crack path due to the presence of platelets is analysed from the point of view of the Coupled Criterion, together with the Matched Asymptotic approach.

Keywords: Finite Fracture mechanics – Coupled Criterion - Micro-scale – Toughening mechanisms

1. Introduction

Glass is increasingly used in structural applications, especially in architecture [1], owing to its numerous advantages: oxidation and corrosion resistance, hardness, and wear resistance. However, the main drawback of glass is its very low fracture toughness. New glass composites have been developed to face this problem. One of these materials is based on the addition of a second constituent,

*Corresponding author. Tel.: +34 627241123
Email address: sara.jimenez_alfaro@sorbonne-universite.fr (S. Jiménez-Alfaro)

with either higher Young's modulus, higher strength, or higher ductility, under the form of platelets, powders, or whiskers. Among others, the first glass composites were developed in 1960 [2].

A good example is the borosilicate glass/Al_2O_3 platelet composite, fabricated by uniaxial hot-pressing, in which alumina platelets are embedded in a borosilicate glass matrix. It was introduced and experimentally characterized by [3]. Since then, multiple studies have been made to explore its capabilities, numerically and experimentally. At first, in [4], residual stresses in the composite were measured by experimentation. Later, they were calculated in a numerical analysis [5]. On the other hand, in [6] and [7] a characterization of the material by means of the roughness in the fracture surface was proposed. Then, new manufacturing processes were described in [8] and [2].

The potential advantage of these composites is the enhancement in the fracture properties with respect to those of the matrix, especially in terms of fracture toughness. It can be noted that different toughening mechanisms were experimentally observed in [6] and [7], such as the penetration of a crack into the platelet, or a deflection. An emphasis will be put in the current analysis on the size effect related to the smallness of these platelets. In this first paper, the toughening mechanisms related to crack propagation interacting with a single platelet is studied.

Hence, the aim of this work is to examine a range of possible toughening mechanisms according to the size effects. The approach is based on Matched Asymptotic Expansions (MAE) and the Coupled Criterion (CC), entering in the framework of Finite Fracture Mechanics (FFM) [9]. Two arguments enter into this CC: an energy and a stress condition. This makes this paper original, it differs significantly from the standard approaches used in general to model these phenomena. In e.g. [10], the authors examine the influence of nanotubes on the stress intensity factor along a crack front located entirely in the matrix. Thus they neglect the direct interaction between the crack and the nanotubes and use a classical Griffith energy argument leaving aside a stress condition. Li and Zhou [11] refer to He and Hutchinson's [12] analysis of a crack deflected

by an interface. The major difference with the present approach lies in the fact that the interface is more or less considered as infinite, i.e. far larger than the crack increment of FFM, statement which is not true in general when the platelet is small [13]. Finally, we can notice [14] where the authors try to answer experimentally to our problematic: "Nano-fillers (nanotubes, nanosheets): do they toughen brittle matrices?"

This paper is divided into 6 sections. In Section 2 material properties are described and the problem is posed. In Sections 3 and 4 the the MA approach and the CC are briefly described. Then, in Section 5 the results are presented, before drawing conclusions in Section refsec:conclusions

2. Description of the problem

In experiments made by [3] and [7] on the borosilicate glass/Al_2O_3 platelet composite, the alumina platelets have hexagonal shape with the major axe measuring $d = 5-25$ μm and the thickness is $t = 0.2\ d$, which means that the dimensions of the platelets are much much smaller than the tested specimens, whose standard cross-section of 12mm^2 has a rectangular shape. Hence, a schematic view of the specimen is shown in Fig. 1. Because of the symmetric 3-point bending loading mode, the pre-existing crack impinging the platelet is under opening mode I. Moreover, as mentioned in [6], the interface between the platelet and the matrix is considered as strong.

Table 1 lists the mechanical properties of the constituents borosilicate glass and Al_2O_3. It is important to emphasize on the high variability of the fracture toughness K_{IC} and the strength σ_{c} of a ceramic material, since they are very dependant on the micro-structure [15]. In this case, these parameters were experimentally obtained for glass in [3] and [7]. However, no experimental data were provided for alumina platelets, being these parameters even more difficult to obtain, since they sometimes differ from the values measured in a bulk material. In [16], a range for σ_{c} was estimated by the values given in the National

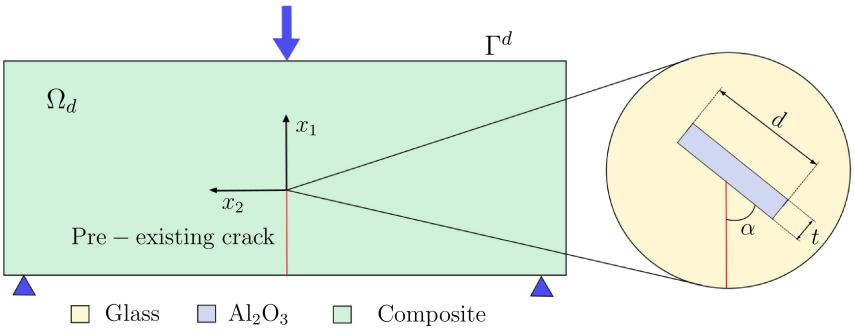

Figure 1: Schematic view of the symmetric 3-point bending test. An alumina platelet with a certain inclination α, is embedded in the glass matrix. The pre-existing crack impinges the platelet.

Institute of Standards and Technology [1]. Furthermore, in [17] a parametric study is proposed, obtaining a possible value for the fracture toughness based on a comparison with experimental observations, among an initial range taken from the literature [18], [19].

Constituents	E [GPa]	ν	α_t [10^{-6}/K]	σ_c [MPa]	K_{IC} [MPa m$^{1/2}$]
Borosilicate glass	60	0.23	3.3	56	0.735
Alumina (Al_2O_3)	402	0.22	8.9	$300 - 400$	$1.7 - 5$

Table 1: Mechanical properties of the constituents.

Notice that in table 1 the thermal coefficients are given. They can be used to obtain the residual stresses generated after manufacture. However, these residual stresses will not be considered in the present analysis mainly focused on the role of the size effect due to the smallness of the inclusion. To that aim, although in the experiments $d = 5 - 25$ μm, the range selected herein is $d = 2 - 300$ μm. For the same purpose, the understanding of the role of smallness, and for simplicity, the analysis is conducted under the assumption of

[1] https://srdata.nist.gov/CeramicDataPortal/Pds/Scdaos

plane strain 2D elasticity.

3. Matched Asymptotic approach

The MA approach [20] provides a two-scale analysis of an elastic problem including a small perturbation in the domain where the problem is posed. This method can be applied if the size of the perturbation is much smaller than the specimen dimensions. In the present case, see Fig. 1, where Ω^d is the actual perturbed domain, the platelet is assumed to be the perturbation, and therefore the initial hypothesis of this methodology is fulfilled. The corresponding elastic displacement is denoted as $\underline{U}^d(x_1, x_2)$. The index d recalls the dependence of the solution to the perturbation. In the framework of MA, $\underline{U}^d(x_1, x_2)$ can be approximated by an outer and an inner expansions. The first one can be written as

$$\underline{U}^d(x_1, x_2) = \underline{U}^0(x_1, x_2) + \text{small correction}, \tag{1}$$

where the leading term $\underline{U}^0(x_1, x_2)$ corresponds to the solution of the same elastic problem settled in the so-called outer domain Ω^0, i.e., assuming the perturbation (the platelet) is too small to be visible in the specimen, and thus, is neglected. This approximation is expected to be relevant far away from the location of the platelet, but becomes meaningless close to it.

In the neighbourhood of the crack tip in Ω_0, the behaviour of $\underline{U}^0(x_1, x_2)$ is described by the Williams' expansion [21], in this case for a crack under Mode I. It is expressed in the polar coordinates system (r, θ) with origin at the crack tip as

$$\underline{U}^0(r, \theta) = \underline{U}^0(0, 0) + K_{\mathrm{I}}\sqrt{r}\underline{u}_I(\theta) + ..., \tag{2}$$

where K_{I} is the stress intensity factor and $\underline{u}(\theta)$ is the opening shape function.

On the other hand, the inner expansion is obtained by a change of variables $x_i = dy_i$ $(i = 1, 2)$ and $r = d\rho$. The assumption of smallness brings us to consider the limit as $d \to 0$, it defines an unbounded domain, called inner domain Ω^{in},

see Fig. 2. The inner expansion is written as

$$\underline{U}^d(x_1, x_2) = \underline{U}^d(dy_1, dy_2) = F_0(d)\underline{V}^0(y_1, y_2) + F_1(d)\underline{V}^1(y_1, y_2) + ... \quad (3)$$

Contrary to the outer expansion, this expression approximates $\underline{U}^d(x_1, x_2)$ in the neighbourhood of the perturbation.

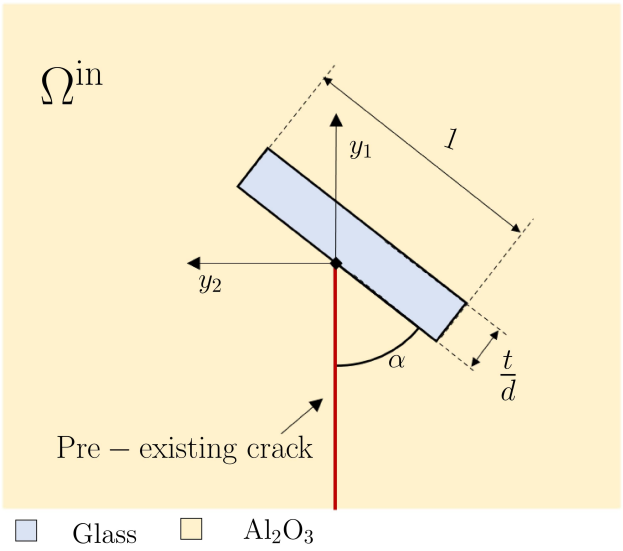

Figure 2: Schematic view of the inner domain. Notice that the length of the alumina platelet is 1.

Since both the inner and the outer expansions are approximations of $\underline{U}^d(x_1, x_2)$, there must be an intermediate region where both solutions coexist, i.e., the solution close to the crack tip in the outer domain must match with the solution far away from the platelet in the inner domain. These are the so-called matching conditions,

$$F_0(d) = 1, \qquad \underline{V}^0(y_1, y_2) \sim \underline{U}^0(0, 0) \qquad \text{when} \qquad \rho \to \infty, \quad (4)$$

$$F_1(d) = K_{\text{I}}\sqrt{d}, \qquad \underline{V}^1(y_1, y_2) \sim \sqrt{\rho}\underline{u}(\theta) \qquad \text{when} \qquad \rho \to \infty, \quad (5)$$

where $\sim$ means "behaves like". From Eq. (4) it is easily seen that $\underline{V}^0(y_1, y_2) = \underline{U}^0(0, 0)$. On the other hand, the solution $\underline{V}^1(y_1, y_2)$ must be numerically cal-

culated in an artificially bounded domain imposing the condition Eq. (5) at a very large distance from the perturbation. To that aim, a Finite Element (FE) simulation is performed using the software FEniCS [22] to numerically obtain the term $\underline{V}^1(y_1, y_2)$ in the inner problem. Notice that, from the theoretical point of view, $\underline{V}^1(y_1, y_2)$ has not a finite energy when $\rho \to \infty$, which means that the solution is not properly determined according to Lax-Milgram theorem. To establish the existence of the solution, a superposition procedure can be followed [20].

The actual solution in the neighbourhood of the platelet is expected to be approximated by the inner expansion. Moreover, the actual stress tensor $\underline{\underline{\sigma}}^d(x_1, x_2)$ is expressed in the vicinity of the perturbation as

$$\underline{\underline{\sigma}}^d(x_1, x_2) = \frac{1}{d}\mathbf{C} : \nabla_y \underline{U}^d(dy_1, dy_2) = \frac{K_{\mathrm{I}}}{\sqrt{d}}\mathbf{C} : \nabla_y \underline{V}^1(y_1, y_2) + ... \qquad (6)$$

where ∇_y denotes the gradient operator with respect to the space variables y_1 and y_2.

In addition, notice that the use of the MA approach allows only one calculation to be made regardless of the actual size of the platelet. In this regard, the strong gradients in the mesh size, needed to solve directly the problem on the actual domain, are avoided, which results in a more accurate solution in the neighbourhood of the perturbation, i.e. the platelet at the crack tip.

4. The Coupled Criterion

The well-known theory of Griffith [23] can only be applied in an homogeneous (at least locally around the crack tip) material or along an interface between homogeneous materials. Moreover, it is easily seen, in [18] for instance, that the CC coincides with Griffith's criterion in these cases and that the stress condition plays no role. In the inner problem an heterogenous micro-structure is considered. Therefore, the theory of Griffith may not be used in all the possible paths for crack propagation that will be studied in the following sections. By applying the CC the stress condition is added to calculate the crack increment.

This criterion, which is generally used to predict the crack nucleation in brittle materials, coincides with the theory of Griffith for crack propagation when the latter can be applied. According to the CC, a crack increment is produced if two necessary and sufficient conditions are simultaneously fulfilled: (i) an energy condition based on an energy balance, and (ii) a stress condition [24].

(i) The energy balance is obtained considering two states of the loaded structure, before and after a crack onset. The change in potential and kinetic energy are denoted as $\Delta\Pi_{\mathrm{p}}$ and $\Delta\Pi_{\mathrm{k}}$ respectively, whereas the fracture energy is defined as $G_{\mathrm{c}}\, S$, being G_{c} a material property and S the newly created crack surface. Hence, the energy balance leads to

$$\Delta\Pi_{\mathrm{p}} + \Delta\Pi_{\mathrm{k}} + G_{\mathrm{c}} S = 0. \tag{7}$$

Which reduces, in a bidimensional problem, to

$$\Delta\Pi_{\mathrm{p}} + \Delta\Pi_{\mathrm{k}} + G_{\mathrm{c}}\delta l = 0, \tag{8}$$

where δl is the newly created crack length (a priori unknown), knowing that Eq. (8) holds per unit thickness of the specimen.

Since the initial state is assumed to be quasi-static, $\Delta\Pi_{\mathrm{k}} \geq 0$, and therefore

$$\Delta\Pi_{\mathrm{p}} + G_{\mathrm{c}}\delta l \leq 0. \tag{9}$$

This can be written as a function of the incremental energy release rate, denoted as $G_{\mathrm{inc}}(\delta l)$,

$$-\frac{\Delta\Pi_{\mathrm{p}}}{\delta l} = G_{\mathrm{inc}}(\delta l) \geq G_{\mathrm{c}}. \tag{10}$$

(ii) The stress condition is based on the tensile strength σ_{c}. The tensile stress σ must be higher than σ_{c} all along the expected crack path. Therefore,

$$\sigma(s) \geq \sigma_{\mathrm{c}}, \qquad \text{for} \qquad 0 \leq s \leq \delta l, \tag{11}$$

where s is the coordinate along the expected crack path.

It is shown in [24] that fracture abruptly occurs from 0 to δl. This incremental form in which a crack of finite size is instantaneously nucleated, is the foundation of Finite Fracture Mechanics (FFM) [9].

Remark: A special care must be brought when the crack is nucleated in a heterogeneous material. Hence, assuming a crack path formed by two segments, one in material A and the other in material B, with different material properties, the energy and stress condition are expressed as a function of the fracture properties of the two materials $G_{\rm c}^{\rm A,\,B}$ and $\sigma_{\rm c}^{\rm A,\,B}$. Thus, Eq. (9) is rewritten as

$$\Delta\Pi_{\rm p} + G_{\rm c}^{\rm A}\delta l^{\rm A} + G_{\rm c}^{\rm B}\delta l^{\rm B} \leq 0, \tag{12}$$

where $\delta l^{\rm A}$ and $\delta l^{\rm B}$ are the newly created crack lengths in materials A and B. Then the energy condition can be written

$$\frac{-\Delta\Pi_{\rm p}}{\delta l^{\rm A} + \delta l^{\rm B}} = G_{\rm inc}(\delta l^{\rm A}, \delta l^{\rm B}) \geq \frac{G_{\rm c}^{\rm A}\delta l^{\rm A} + G_{\rm c}^{\rm B}\delta l^{\rm B}}{\delta l^{\rm A} + \delta l^{\rm B}}. \tag{13}$$

On the other hand, Eq. (11) splits into two conditions, described as

$$\sigma(s) \geq \sigma_{\rm c}^{\rm A}, \qquad \text{for} \qquad 0 \leq s \leq \delta l^{\rm A}, \tag{14}$$

$$\sigma(s) \geq \sigma_{\rm c}^{\rm B}, \qquad \text{for} \qquad \delta l^{\rm A} \leq s \leq \delta l^{\rm A} + \delta l^{\rm B}. \tag{15}$$

In order to apply the CC, the actual elastic solution at the vicinity of the crack tip is estimated from the inner expansion. Thus, the incremental energy release rate in the inner problem $G_{\rm inc}^{\rm in}(\delta l)$ is numerically calculated releasing one by one the set of pair of nodes of the Finite Element mesh along the supposed crack path. For each released pair of nodes, $\delta l^{\rm in}$ is the distance from that node to the origin expressed in the dimensionless y_i variables. Then, $G_{\rm inc}^{d}(\delta l)$ is estimated by

$$G_{\rm inc}^{d}(\delta l) = \frac{-\Delta\Pi_{\rm p}^{d}(\delta l)}{\delta l}, \tag{16}$$

where

$$\Delta\Pi_{\rm p}^{d}(\delta l) = \Delta W^{d}(\delta l), \tag{17}$$

being $W^{d}(\delta l)$ the strain energy in the system, defined as

$$W^{d}(\delta l) = \frac{1}{2}\int_{\Omega^{d}} \mathbf{C} : \nabla_x \underline{U}^{d} : \nabla_x \underline{U}^{d} dx_1 dx_2. \tag{18}$$

Among the two states considered in $\Delta W^{d}(\delta l) = W^{d}(\delta l) - W^{d}(0)$, only the crack is changing in the solid. Therefore, $\Delta W^{d}(\delta l)$ can be approximated by the inner

expansion, $\Delta W^d(\delta l) = d\,\Delta W^{\text{in}}(\delta l^{\text{in}})$, where

$$W^{\text{in}}(\delta l^{\text{in}}) = \frac{1}{2}\int_{\Omega^{\text{in}}} \mathbf{C} : \nabla_y \underline{V}^1 : \nabla_y \underline{V}^1 dy_1 dy_2, \tag{19}$$

and $\delta l^{\text{in}} = \frac{\delta l}{d}$ is the dimensionless newly created crack length in the inner domain Ω^{in}. Thus, Eq. (19) is numerically obtained and the incremental energy release rate is approximated as

$$G^d_{\text{inc}}(\delta l) = \frac{d\,\Delta W^{\text{in}}(\delta l^{\text{in}})}{d\,\delta l^{\text{in}}} = \frac{\Delta W^{\text{in}}(\delta l^{\text{in}})}{\delta l^{\text{in}}}, \tag{20}$$

where it is observed that $G^d_{\text{inc}}(\delta l)$ does not depend on the length of the platelet, d.

The apparent fracture toughness, $K^{\text{app}}_{\text{IC}}$ is taken as the minimum value of K_I for which both the energy and the stress conditions are fulfilled, among all the possible studied crack paths. The aim is to analyse the different factors that could increase $K^{\text{app}}_{\text{IC}}$, compared to the fracture toughness K_{IC} of glass.

5. Analysis of toughening mechanisms

In the following sub-sections the equivalent 2D model presented in Section 3 is considered to numerically determine the apparent fracture toughness $K^{\text{app}}_{\text{IC}}$ of the composite, as a function of d and α. Three different orientations are presented in this paper, $\alpha = 0°, 45°, 90°$. For the sake of simplicity, the superscript d related to the actual solution in Section 3, is omitted in the notation. Furthermore, K^{g}_{IC}, $\sigma^{\text{g}}_{\text{c}}$ denote the fracture properties of glass, and K^{a}_{IC}, $\sigma^{\text{a}}_{\text{c}}$ those of alumina.

5.1. Results for $\alpha = 0°$

When $\alpha = 0°$, the platelet is parallel to the pre-existing crack and we assume the crack to impinge the platelet at its corner. In that case, only one crack path seems likely to occur, it is the one located along the interface between glass and alumina, see Fig. 3. As it was already mentioned, the interface is considered as strong [7], therefore its fracture properties are those of glass.

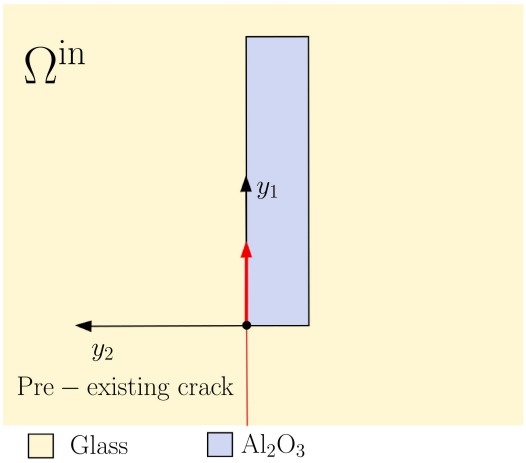

Figure 3: Schematic view of the inner domain for $\alpha = 0°$. The supposed crack path starts from the corner of the platelet (red arrow).

The dependence of $K_{\text{IC}}^{\text{app}}$ on the size of the platelet is represented in Fig 4, where it is shown that K_{IC}^{g} is enhanced only if $d > 50$ μm. However, if $d < 50$ μm, then $K_{\text{IC}}^{\text{app}} < K_{\text{IC}}^{\text{g}}$. It can be explained by the stress singularities located at the corners of the platelet. The effect of these singularities, i.e. very high stresses that tend to infinity at the corners, is felt all along the face of the platelet if it is small.

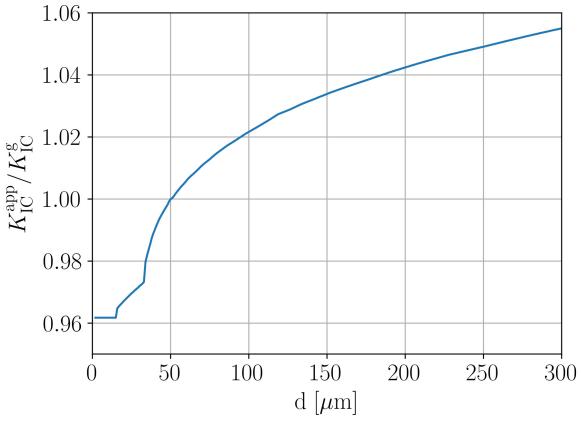

Figure 4: Evolution of $K_{\text{IC}}^{\text{app}}/K_{\text{IC}}^{\text{g}}$ with respect to d, for $\alpha = 0°$.

According to the CC, a finite crack increment develops in an unstable manner. For $d = 16 - 33$ μm this length is equal to the length of the glass/alumina interface ($x_1 = d$), while for $d > 33$ μm this finite jump becomes smaller than the interface length, and the presence of the stiff material increasingly diminishes the ability of the crack to open. Moreover, it is observed that if $d < 16$ μm, the apparent fracture toughness remains constant, since the evolution of the failure is governed by the energy condition, and G_{inc} does not depend on d, see Section 4.

As an example, in Fig. 5a the CC is analysed for $d = 10$ μm. In the graphic, the superscript i represents either g or a. It should be noted that there is a small peak in the stress condition at the end of the interface ($x_1 = 10$), due to the singularity at the corner point. Furthermore, notice that this is a non standard result of the CC, which is baptized as negative geometry [25], since the energy curve is not an increasing function in the glass region. Other examples of the application of the CC are given in Fig. 5b for $d = 20$ μm and Fig. 5c, for $d = 100$ μm.

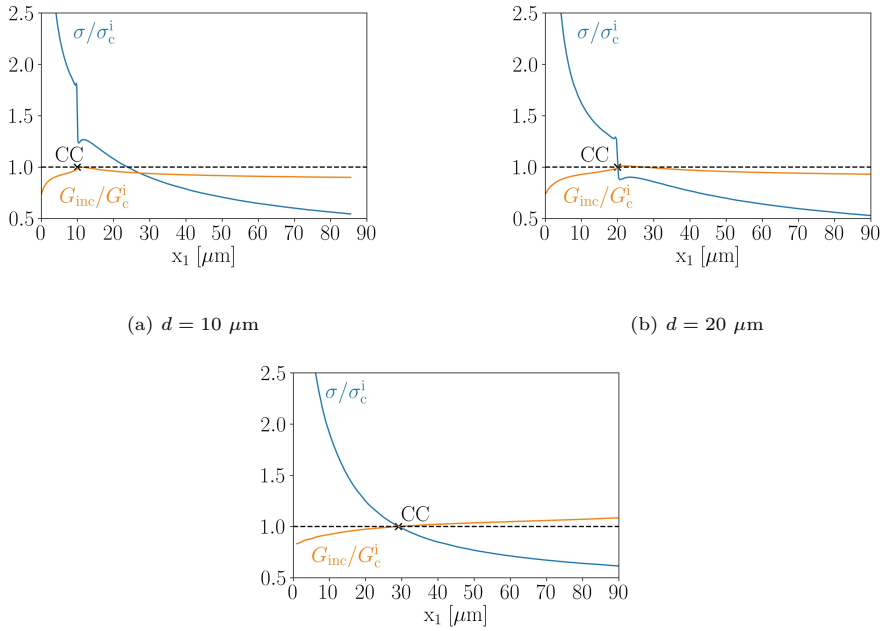

(a) $d = 10$ μm

(b) $d = 20$ μm

(c) $d = 100$ μm

Figure 5: Examples of the application of the CC for $\alpha = 0°$.

5.2. Results for $\alpha = 90°$

Another relative position of the platelet is given when it is perpendicular to the pre-existing crack, $\alpha = 90°$. Since a priori the crack path is unknown, different options are investigated, studied in the following subsections.

5.2.1. Single deflection, decohesion and step over

This section describes the analysis made by the CC on different examples, for those possible crack paths where fracture properties of glass determine the evolution of the failure.

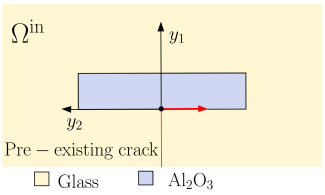

(a) Deflection

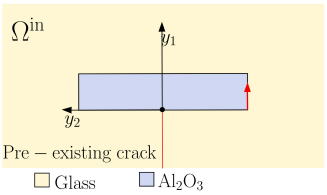

(b) Decohesion

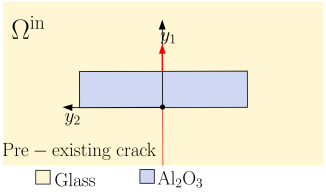

(c) Step over

Figure 6: Scheme of the inner domain and the supposed crack path (red arrow) for $\alpha = 90°$, for different toughening mechanisms.

A first option is given when the crack encounters the platelet and deflects along the interface, as shown in Fig. 6a. Another possible mechanism is a lateral decohesion of the interface, see Fig. 6b. Finally, the situation in which the crack reinitiates on the opposite face of the platelet, leading to a nucleation in the glass region, has also been studied. It is called the step over case, represented in Fig. 6c. This kind of mechanism can be met in rock mechanics for instance [26]. However, results have shown that it is not a relevant mechanism in the present case, since the apparent fracture toughness obtained for this case is much higher than the ones obtained for the rest of the cases. Therefore, it is not likely to happen in the material under study.

Firstly, in Fig. 7 an example of the crack deflection is explained, for $d = 50$ μm. The stress condition is a decreasing function, whereas the energy curve is increasing with x_1. It is shown that the newly created crack length is shorter than the interface length.

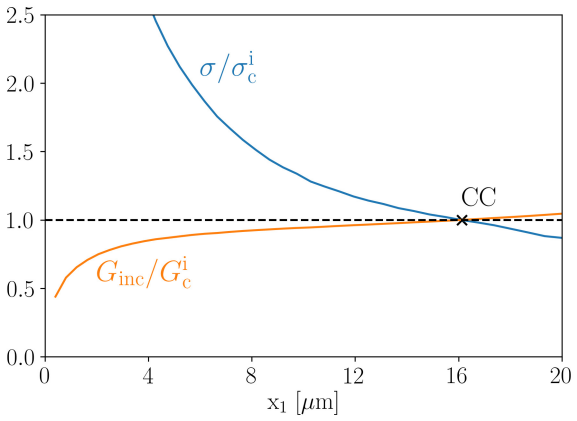

Figure 7: Application of the CC for $\alpha = 90°$ in the case of deflection, shown in Fig. 6a, for $d = 50$ μm.

It is important to highlight that the case of a double symmetric deflection can also be studied even in a simpler way considering a half of the domain in the problem, and applying the corresponding symmetry conditions. Although both a single and a double symmetric deflection were studied, no significant differences have been observed between the two cases, as it was done in [27]. For this reason, in this paper only the results for a single deflection are presented.

On the other hand, two examples are given for $d = 100$ μm and $d = 200$ μm in Figs. 8a and 8b, respectively. In the first case, $d = 100$ μm, the crack grows until the end of the lateral interface glass/alumina. In the second case, $d = 200$ μm, the crack jump is bigger and the initiation length ends in the glass region.

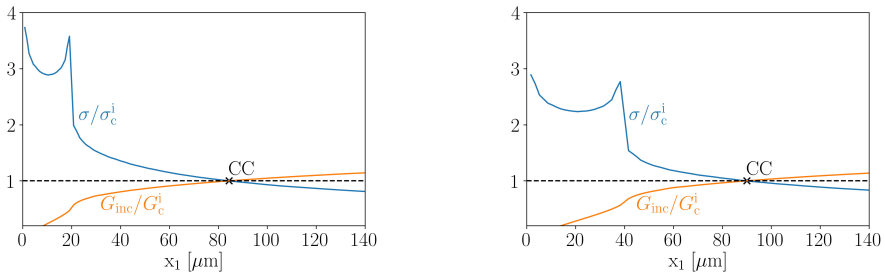

(a) $d = 100$ μm

(b) $d = 200$ μm

Figure 8: Application of the CC for $\alpha = 90°$ in the case of decohesion, shown in Fig. 6b.

5.2.2. Penetration

205 A separate case in which the crack penetrates in the platelet is presented in Fig. 9, in which the fracture properties of Al_2O_3, defined through a range of possible values, determine the evolution of the failure.

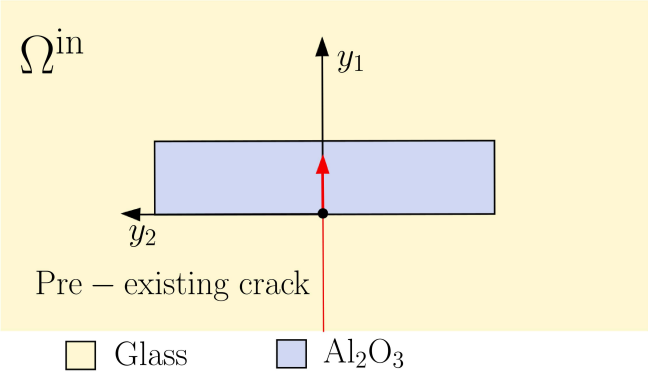

Figure 9: Scheme of the inner domain and the supposed crack path (red arrow) for $\alpha = 90°$ and penetration.

In Fig. 10 the function $K_{IC}^{app}(d)$ is studied for the range of σ_c^a. It is observed that the apparent fracture toughness is increased with the strength of alumina

and the size of the platelet.

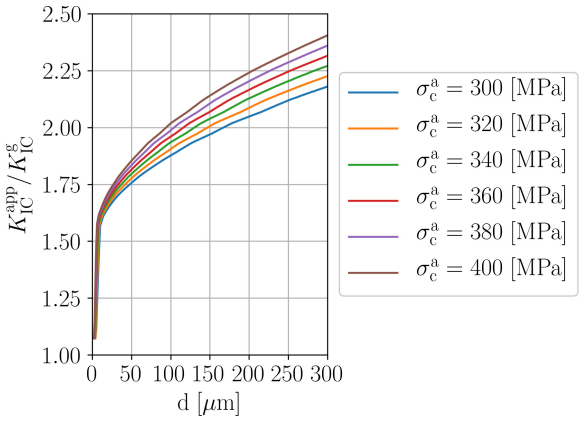

Figure 10: Evolution of K_{IC}^{app}/K_{IC}^{g} with d for several values of σ_c^a in the case of a crack penetration, considering an average value of the fracture toughness $K_{IC}^{a} = 3.35$ MPa $\cdot$ m$^{1/2}$.

On the other hand, Fig. 11 shows that the influence of K_{IC}^{a} on the apparent fracture toughness is more significant when d is increased. As a general remark, the greater the fracture properties of alumina, the greater values of $K_{IC}^{app}(d)$ given in the composite.

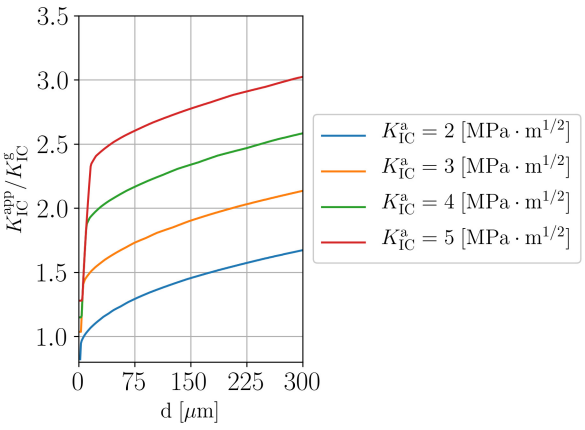

Figure 11: Evolution of K_{IC}^{app}/K_{IC}^{g} with d for several values of K_{IC}^{a} in the case of a crack penetration, considering an average value of the strength $\sigma_c^a = 350$ MPa.

As an example, a description of the CC for $K_{\mathrm{IC}}^{\mathrm{a}} = 2$ MPa$\cdot$m$^{1/2}$ and $\sigma_{\mathrm{c}}^{\mathrm{a}} = 300$ MPa is given in Fig. 12, where two cases are shown. In Fig. 12a the crack propagates inside the alumina platelet, whereas in Fig. 12b a more standard fulfillement of the CC is represented, for a longer platelet.

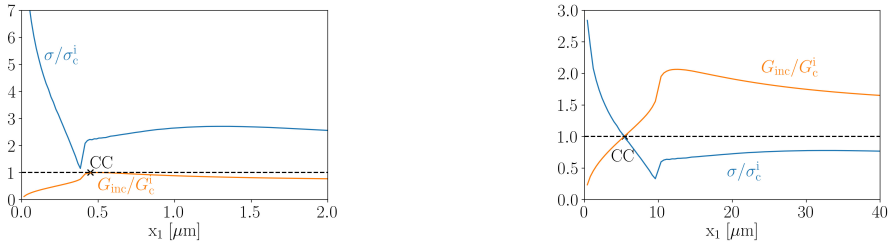

(a) $d = 2$ μm

(b) $d = 50$ μm

Figure 12: Application of the CC for $\alpha = 90°$ in the case of penetration, shown in Fig. 9, considering $K_{\mathrm{IC}}^{\mathrm{a}} = 2$ MPa $\cdot$ m$^{1/2}$ and $\sigma_{\mathrm{c}}^{\mathrm{a}} = 300$ MPa.

5.2.3. Comparison between mechanisms

Finally, in Fig. 13 the expected crack paths presented in Sections 5.2.1 and 5.2.2 are compared to determine the predominant toughening mechanism, which is the one associated with the lowest $K_{\mathrm{IC}}^{\mathrm{app}}$, i.e. with the lowest critical load. For the sake of simplicity, only two cases are chosen for penetration, corresponding to the most extreme values of the Al_2O_3 fracture properties, given in table 1. The minor case, in which $K_{\mathrm{IC}}^{\mathrm{a}} = 2$ MPa $\cdot$ m$^{1/2}$, $\sigma_{\mathrm{c}}^{\mathrm{a}} = 300$ MPa, and the major case, where $K_{\mathrm{IC}}^{\mathrm{a}} = 5$ MPa$\cdot$m$^{1/2}$, $\sigma_{\mathrm{c}}^{\mathrm{a}} = 400$ MPa. Notice that they constitute an upper and a lower bound in the curves given in Fig. 13 for the case of penetration. It is observed that the major case is never predominant. Moreover, for very short platelets the predominant mechanism is the penetration. Then, if $d > 6$ μm the predominant mechanism depends on the fracture properties of Al_2O_3, and it can be either a decohesion, either a penetration. Finally, for long platelets $d > 160$ μm a deflection through the interface glass/alumina or a penetration can occur, depending, again, on the fracture properties of alumina.

In 1989, He and Hutchinson [12] explained the necessary condition for a crack

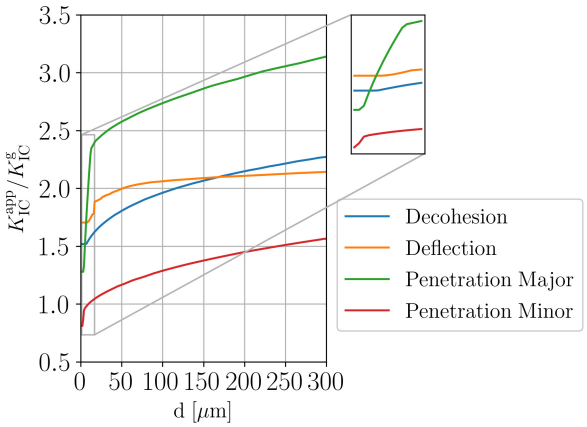

Figure 13: Evolution of $K_{\mathrm{IC}}^{\mathrm{app}}/K_{\mathrm{IC}}^{\mathrm{g}}$ with respect to the length of the platelet d, for a single deflection, a decohesion and a penetration, when $\alpha = 90°$.

to either penetrate or deflect through the interface of a semi-infinite domain divided into two phases, in this case, glass and alumina, with a pre-existing crack in glass. For a right angle, H&H's condition for a crack to be deviated is

$$\frac{G_{\mathrm{c}}^{\mathrm{g}}}{G_{\mathrm{c}}^{\mathrm{a}}} < \frac{G_{\mathrm{p}}}{G_{\mathrm{d}}}, \tag{21}$$

whereas it penetrates in the reverse situation. The energy release rate related to deflection and penetration are denoted as G_{d} and G_{p} respectively. In [13] this ratio is expressed in terms of the asymptotic solution, as a function dependant on the ratio $E^{\mathrm{a}}/E^{\mathrm{g}}$. In the bi-material case studied this ratio $E^{\mathrm{a}}/E^{\mathrm{g}} = 1.902$. Hence, $G_{\mathrm{d}}/G_{\mathrm{p}} = 0.68$.

Two different values of $G_{\mathrm{c}}^{\mathrm{a}}$ are considered, the upper and lower bound of the alumina fracture toughness, see table 1. Hence, according to H&H, for $K_{\mathrm{IC}}^{\mathrm{a}} = 2$ MPa $m^{1/2}$ the ratio $G_{\mathrm{c}}^{\mathrm{g}}/G_{\mathrm{c}}^{\mathrm{a}} = 0.906$ and the crack will penetrate, whereas for $K_{\mathrm{IC}}^{\mathrm{a}} = 5$ MPa $m^{1/2}$ the ratio $G_{\mathrm{c}}^{\mathrm{g}}/G_{\mathrm{c}}^{\mathrm{a}} = 0.145$ and it will deflect.

In Fig. 13, the numerical toughening mechanisms studied for $\alpha = 90°$ were compared. If $K_{\mathrm{IC}}^{\mathrm{a}} = 2$ MPa $m^{1/2}$, the penetration clearly predomines. However, if $K_{\mathrm{IC}}^{\mathrm{a}} = 5$ MPa $m^{1/2}$, the predominant mechanism is the deflection for $d < 160$ μm and the decohesion if $d > 160$ μm. This observation agrees with

the theoretical results, since they refer to a semi-infinite domain, which would correspond to the case of very large platelets.

5.3. Results for $\alpha = 45°$

In the case $\alpha = 45°$ two more parameters are used to define the expected crack path, as illustrated in Fig. 14. The angle β, the first deflection angle of the crack when it penetrates in the alumina platelet, and the angle γ, a secondary deflection when the prescribed crack penetrates from the alumina platelet to the glass matrix. To differentiate the possible toughening mechanisms that can be given in this situation, three possible values for each angle, $\beta, \gamma = 0°, 45°$ and $90°$, are studied.

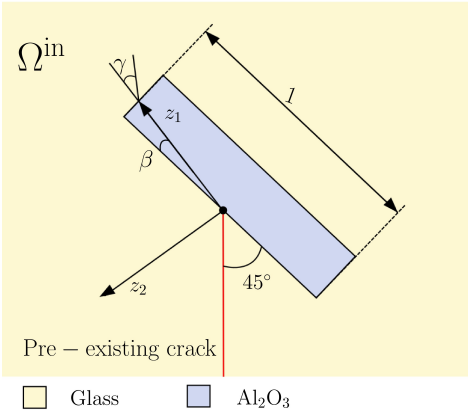

Figure 14: Scheme of the expected crack path in the inner problem for $\alpha = 45°$. A new local coordinates system is defined (z_1, z_2), so that z_1 is always oriented with the supposed crack path.

5.3.1. Toughening mechanisms: case $\beta = 0°$

If $\beta = 0°$ a deflection of the crack along the interface glass/alumina occurs. When the crack reaches the end of the platelet, a second deflection is possible, defined by $\gamma = 0°, 45°, 90°$, see Figs.15a-15b.

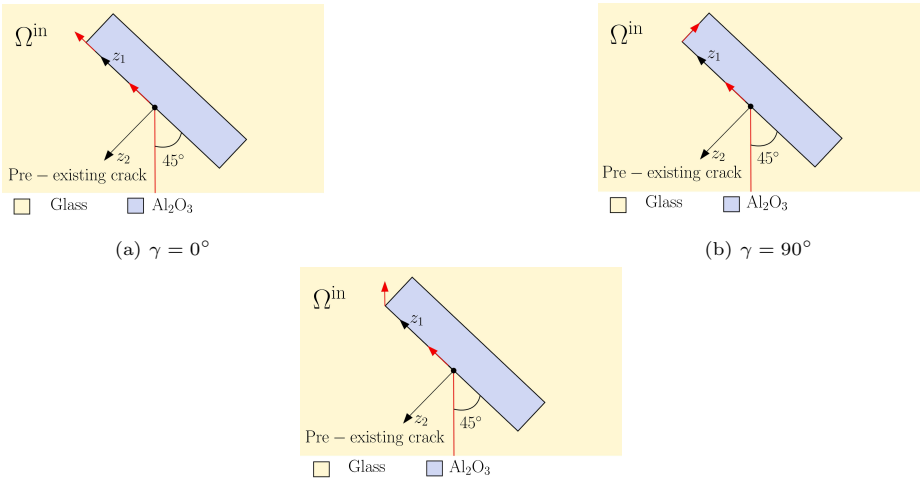

(a) $\gamma = 0°$

(b) $\gamma = 90°$

(c) $\gamma = 45°$

Figure 15: Scheme of the inner domain for $\alpha = 45°$ and $\beta = 0°$ and the supposed crack paths (red arrows).

The predominant crack path is obtained by comparing the apparent fracture toughness of the three options, see Fig. 16.

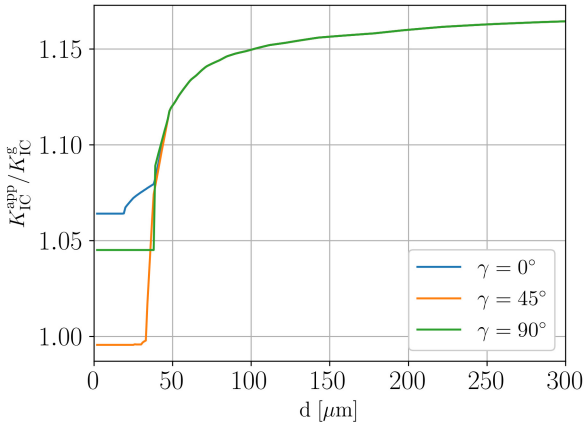

Figure 16: Evolution of $K_{\mathrm{IC}}^{\mathrm{app}}/K_{\mathrm{IC}}^{\mathrm{g}}$ with d for several values of γ in the case of $\beta = 0°$.

It is observed that for $d > 47$ μm there is no difference among the three possibilities, since the crack increment is produced along the glass/alumina in-

terface. Furthermore, below $d = 47$ μm, $\gamma = 45°$ predomines. It should be noted that for short platelets $K_{\mathrm{IC}}^{\mathrm{app}}(d)$ remains constant, since it is the energy condition the one that is governing the failure.

5.3.2. Toughening mechanisms: case of $\beta = 90°$ and $\beta = 45°$

In Fig. 17 the three expected paths analysed for $\beta = 90°$ are presented. Once the crack penetrates into the platelet it can be deflected through the interface glass/alumina ($\gamma = 0°$), or it can be propagated in the glass region, following the same direction as the pre-existing crack ($\gamma = 45°$) or the same direction as it had when it entered in the alumina ($\gamma = 90°$).

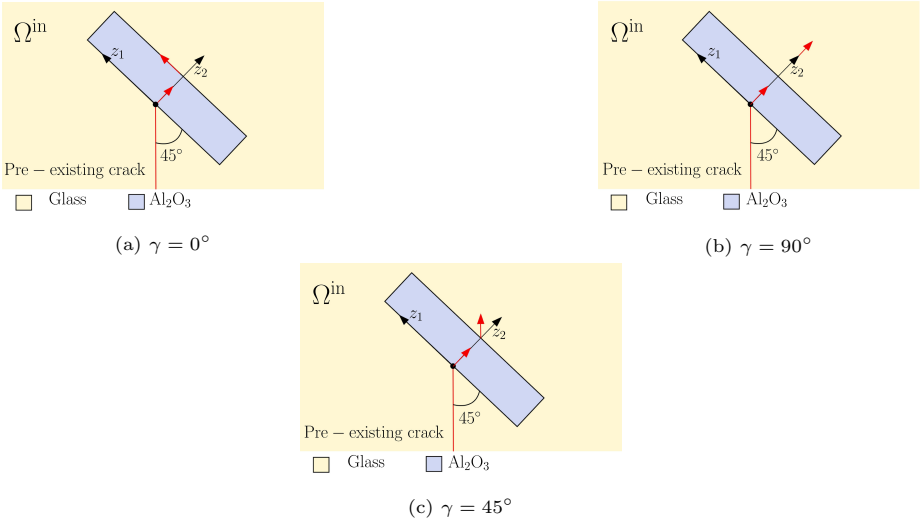

(a) $\gamma = 0°$

(b) $\gamma = 90°$

(c) $\gamma = 45°$

Figure 17: Scheme of the inner domain for $\alpha = 45°$ and $\beta = 90°$ and the supposed crack paths (red arrows).

In Fig. 18 the three expected crack paths are compared, where the so-called major and minor cases were described in Section 5.2.3. As it was observed for other cases, different behaviours can be distinguished. They are related to the different results arised by the CC analysis. A zoom inside each graph highlights the region of short platelets. Clearly, when the fracture properties of alumina are improving, $K_{\mathrm{IC}}^{\mathrm{app}}$ is increasing. In fact, for very short platelets it is observed

that the crack deflection for the minor case is not enough to increase $K_{\mathrm{IC}}^{\mathrm{app}}$ with respect to $K_{\mathrm{IC}}^{\mathrm{g}}$ for very low values of the alumina fracture properties.

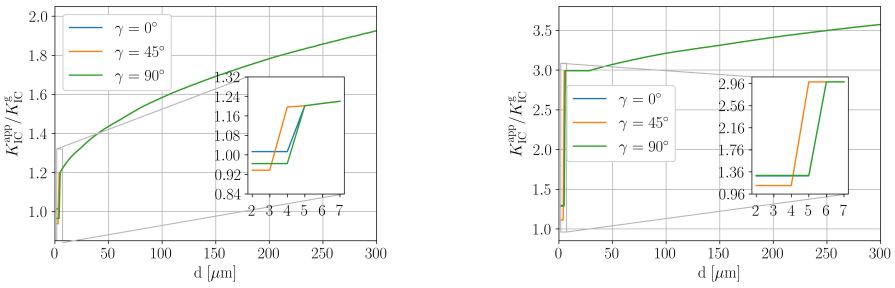

(a) Minor case

(b) Major case

Figure 18: Evolution of $K_{\mathrm{IC}}^{\mathrm{app}}/K_{\mathrm{IC}}^{\mathrm{g}}$ with d for several values of γ in the case of $\beta = 90°$.

On the other hand, Fig. 19 shows the three possible crack paths analysed for the case of $\beta = 45°$, i.e. when the crack penetrates straight into the platelet.

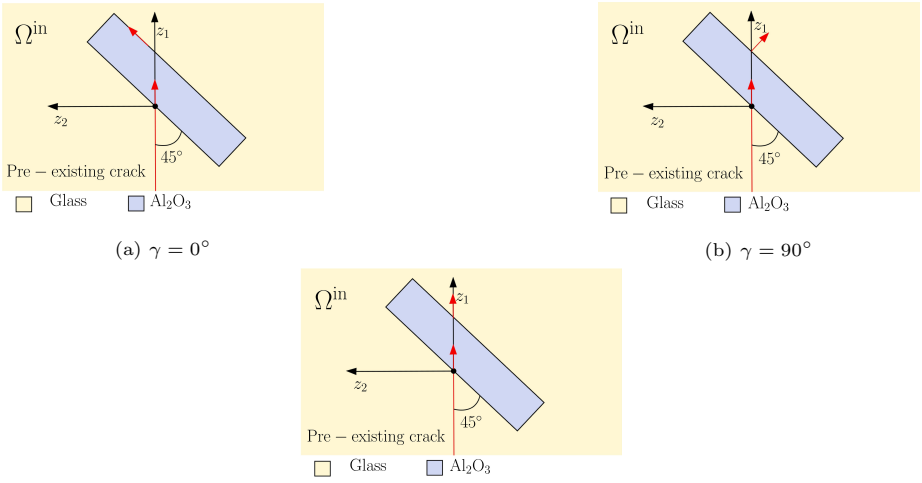

(a) $\gamma = 0°$

(b) $\gamma = 90°$

(c) $\gamma = 45°$

Figure 19: Scheme of the inner domain for $\alpha = 45°$ and $\beta = 45°$ and the expected crack paths (red arrows).

In Fig. 20, conclusions are very similar to the two previous cases, where $\gamma = 45°$ remains the most probable case, i.e. the predominant mechanism, for

both the minor and the major examples. Again, there are only differences in the short platelets.

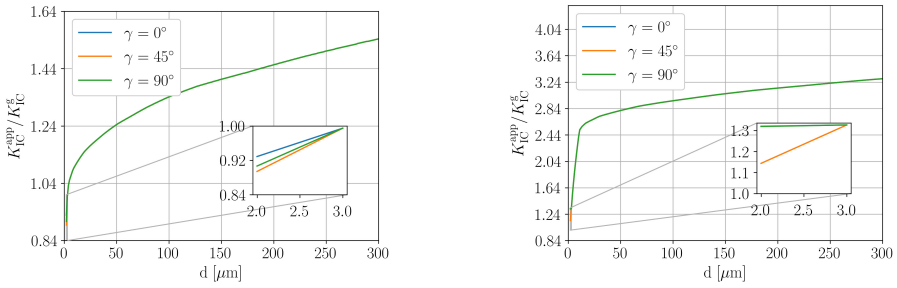

(a) Minor case

(b) Major case

Figure 20: Evolution of K_{IC}^{app}/K_{IC}^{g} with d for several values of γ in the case of $\beta = 45°$.

Finally, a comparison is made for the minor and major case for the three β angles. As it can be seen, the predominant path depends on the alumina fracture properties. In the major case, in general, it is the deflection $\beta = 0°$ across the interface glass/alumina that predominates, but not for very short platelets, where the crack is expected to penetrate into the platelet, having a deflection with respect to its original orientation, case of $\beta = 90°$. On the other hand, in the minor case, the crack penetrates into the platelet without suffering any change in its orientation, i.e., $\beta = 45°$.

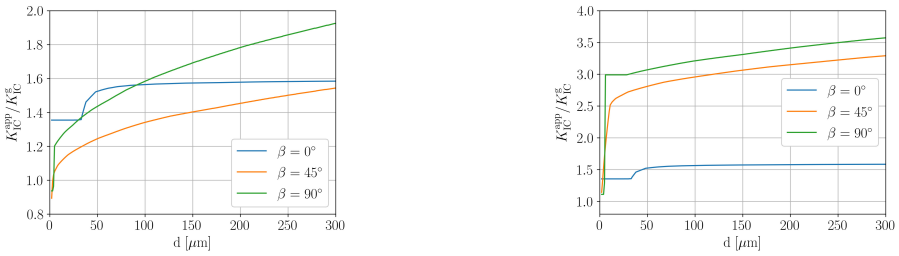

(a) $K_{IC}^{al} = 2$ MPa $\cdot$ m$^{1/2}$ and $\sigma_c^{al} = 300$ MPa

(b) $K_{IC}^{al} = 5$ MPa $\cdot$ m$^{1/2}$ and $\sigma_c^{al} = 400$ MPa

Figure 21: Evolution of K_{IC}^{app}/K_{IC}^{g} with d for several values of β.

6. Conclusions

As a general conclusion, a size effect is observed. When the length of the platelet is very small, it is the energy condition that is governing the failure, and consequently the apparent fracture toughness remains constant. Notice that similar conclusions were also observed for bending tests on microcantilever beams at the micro-scale in [28]. The size of the platelet d plays also a role on the newly created crack length. If the platelet is short, the crack evolves in an unstable manner joining the glass region beyond the platelet, whereas if it is long, the crack increment remains inside the platelet, or along the interface glass/alumina.

Moreover, in some cases with very short platelets, as $\alpha = 0°$, a change in the crack path is not enough to enhance the apparent fracture toughness. It means that other toughening mechanisms should be invoked for improving $K_{\mathrm{IC}}^{\mathrm{app}}$, such as a significant increase in the mechanical properties.

The influence of the alumina fracture properties on the toughening mechanisms has been analysed. It can be concluded that both $K_{\mathrm{IC}}^{\mathrm{a}}$ and $\sigma_{\mathrm{c}}^{\mathrm{a}}$ have an impact on the composite fracture properties. However, $K_{\mathrm{IC}}^{\mathrm{a}}$ has a greater influence on $K_{\mathrm{IC}}^{\mathrm{app}}$.

Some simplifications have been made in this paper. One of them is that only several representative examples of the expected crack path were analysed. This analysis could be complemented by a first calculation of the expected crack path among all the numerous possibilities, for example, using the Phase Field methodology, assumming much higher computational costs.

This paper constitutes the first half of the study. In a second part [29], the role of multiple platelets will be considered, by introducing a surrounding homogeneous equivalent material, whose properties are obtained from experimental results found in the literature. On the other hand, the effect of residual stresses will be analysed. They are produced during cooling after the manufacturing process, where the temperature exceeds $500°C$. It is important to highlight that a separate analysis of these three toughening mechanisms (the deviation of

the crack path, the improvement of the material properties, and the presence of residual stresses) is a key tool for an optimal material design, since it allows to study their individual contribution to enhance the material fracture properties. Furthermore, this individual analysis is much more difficult to obtain through experiments.

Acknowledgments

The funding received from the European Union's Horizon 2020 research and innovation programme under Marie Skłodowska-Curie grant agreement No. 861061- NEWFRAC is gratefully acknowledged.

References

[1] J. Schneider, S. Schula, W. Weinhold, Characterisation of the scratch resistance of annealed and tempered architectural glass, Thin solid Film 520 (2012) 4190–4198. doi:http://dx.doi.org/10.1016/j.tsf.2011.04.104.

[2] E. Bernardo, R. Castellan, , S. Hreglich, Al2o3-platelet reinforced glass matrix composites from a mixture of wastes. journal of materials science, Journal of materials science 42 (8) (2007) 2706–2711. doi:https://doi.org/10.1007/s10853-006-1378-8.

[3] A. R. Boccaccini, P. A. Trusty, Toughening and strengthening of glass by al203 platelets, Journal of materials science letters 15 (1) (1996) 60–63. doi:https://doi.org/10.1007/BF01855614.

[4] R. Todd, A. Boccaccini, R. Sinclair, R. Yallee, R. Young, Thermal residual stresses and their toughening effect in al2o3 platelet reinforced glass, Acta materialia 47 (11) (1999) 3233–3240. doi:https://doi.org/10.1016/S1359-6454(99)00177-9.

[5] V. Cannillo, C. Leonelli, A. R. Boccaccini, Numerical models for thermal residual stresses in al2o3 platelets/borosilicate glass matrix composites, Materials Science and Engineering: A 323 (1-2) (2002) 246–250. doi:https://doi.org/10.1016/S0921-5093(01)01345-4.

[6] A. Boccaccini, V. Winkler, Fracture surface roughness and toughness of al2o3-platelet reinforced glass matrix composites, Composites Part A: Applied Science and Manufacturing 33 (1) (2002) 125–131. doi:https://doi.org/10.1016/S1359-835X(01)00080-X.

[7] M. Kotoul, J. Pokluda, P. Šandera, I. Dlouhỳ, Z. Chlup, A. Boccaccini, Toughening effects quantification in glass matrix composite reinforced by alumina platelets, Acta materialia 56 (12) (2008) 2908–2918. doi:https://doi.org/10.1016/j.actamat.2008.02.024.

[8] E. Bernardo, G. Scarinci, Sintering behaviour and mechanical properties of al2o3 platelet-reinforced glass matrix composites obtained by powder technology, Ceramics international 30 (5) (2004) 785–791. doi:http://dx.doi.org/10.1016/j.ceramint.2003.09.013.

[9] Z. Hashin, Finite thermoelastic fracture criterion with application to laminate cracking analysis, Journal of the Mechanics and Physics of Solids 44 (7) (1996) 1129–1145. doi:http://dx.doi.org/10.1016/0022-5096(95)00080-1.

[10] D. Ali, S. Sen, Finite element analysis of boron nitride nanotubes' shielding effect on the stress intensity factor of semielliptical surface crack in a wide range of matrixes using rve model, Composites Part B: Engineering 110 (2017) 351–360. doi:https://doi.org/10.1016/j.compositesb.2016.11.017.

[11] Y. Li, M. Zhou, Prediction of fracturess toughness of ceramic composites as function of microstructure: Ii. analytical model, Journal of the Mechanics and Physics of Solids 61 (2) (2013) 489–503. doi:https://doi.org/10.1016/j.jmps.2012.09.011.

[12] M.-Y. He, J. W. Hutchinson, Crack deflection at an interface between dissimilar elastic materials, International journal of solids and structures 25 (9) (1989) 1053–1067. doi:https://doi.org/10.1016/0020-7683(89)90021-8.

[13] D. Leguillon, E. Martin, Crack nucleation at stress concentration points in composite materials—application to crack deflection by an interface, in: Mathematical Methods and Models in Composites, 2014, pp. 401–424. doi:https://doi.org/10.1142/9781848167858_0010.

[14] I. Dlouhy, P. Tatarko, L. Bertolla, Z. Chlup, Nano-fillers (nanotubes, nanosheets): do they toughen brittle matrices?, Procedia Structural Integrity 23 (2019) 431–438. doi:https://doi.org/10.1016/j.prostr.2020.01.125.

[15] R. Danzer, On the relationship between ceramic strength and the requirements for mechanical design, Journal of the European Ceramic Society 34 (15) (2014) 3435–3460. doi:http://dx.doi.org/10.1016/j.jeurceramsoc.2014.04.026.

[16] V. Cannillo, G. Pellacani, C. Leonelli, A. Boccaccini, Numerical modelling of the fracture behaviour of a glass matrix composite reinforced with alumina platelets, Composites Part A: Applied Science and Manufacturing 34 (1) (2003) 43–51. doi:https://doi.org/10.1016/S1359-835X(02)00230-0.

[17] V. Cannillo, A. Corradi, C. Leonelli, A. Boccaccini, A simple approach for determining the in situ fracture toughness of ceramic platelets used in composite materials by numerical simulations, Journal of materials science letters 20 (20) (2001) 1889–1891. doi:https://doi.org/10.1023/A:1012870110675.

[18] A. G. Evans, E. A. Charles, Fracture toughness determinations by indentation, Journal of the American Ceramic society 59 (7-8) (1979) 371–372. doi:https://doi.org/10.1111/j.1151-2916.1976.tb10991.x.

[19] G. Anstis, P. Chantikul, B. R. Lawn, D. Marshall, A critical evaluation of indentation techniques for measuring fracture toughness: I, direct crack measurements, Journal of the American Ceramic Society 64 (9) (1981) 533–538. doi:https://doi.org/10.1111/j.1151-2916.1981.tb10320.x.

[20] D. Leguillon, E. Sanchez-Palencia, Computation of singular solutions in elliptic problems and elasticity, 1987. doi:https://doi.org/10.1002/zamm.19880681137.

[21] M. L. Williams, Stress singularities resulting from various boundary conditions in angular corners of plates in extension, Journal of Applied Mechanics 19 (4) (1952) 526–528. doi:http://dx.doi.org/10.1115/1.4010553.

[22] H. P. Langtangen, A. Logg, Solving PDEs in Python, Springer, 2017. doi:10.1007/978-3-319-52462-7.

[23] A. A. Griffith, VI. the phenomena of rupture and flow in solids, Philosophical transactions of the royal society of london. Series A, containing papers of a mathematical or physical character 221 (582-593) (1921) 163–198. doi:https://doi.org/10.1098/rsta.1921.0006.

[24] D. Leguillon, Strength or toughness? a criterion for crack onset at a notch, European Journal of Mechanics - A/Solids 21 (1) (2002) 61–72. doi:https://doi.org/10.1016/S0997-7538(01)01184-6.

[25] P. Weißgraeber, S. Hell, W. Becker, Crack nucleation in negative geometries, Engineering Fracture Mechanics 168 (2016) 93–104, modeling of fracture and damage in composite materials. doi:https://doi.org/10.1016/j.engfracmech.2016.02.045.

[26] D. Quesada, D. Picard, C. Putot, D. Leguillon, The role of the interbed thickness on the step-over fracture under overburden pressure, International Journal of Rock Mechanics and Mining Sciences 46 (2) (2009) 281–288. doi:http://dx.doi.org/10.1016/j.ijrmms.2008.04.006.

[27] I. García, V. Mantič, E. Graciani, Debonding at the fibre–matrix interface under remote transverse tension. one debond or two symmetric debonds?, European Journal of Mechanics-A/Solids 53 (2015) 75–88. doi:http://dx.doi.org/10.1016/j.euromechsol.2015.02.007.

[28] S. Jiménez-Alfaro, D. Leguillon, Finite fracture mechanics at the micro-scale. application to bending tests of micro cantilever beams, Engineering Fracture Mechanics 258 (2021) 108012. doi:https://doi.org/10.1016/j.engfracmech.2021.108012.

[29] S. Jiménez-Alfaro, D. Leguillon, Modeling of glass reinforced matrices by the coupled criterion. part ii: role of the residual stresses and multiple platelets. in preparation.